Optical trapping of polystyrene beads in mixed solvents

Optical trapping of polystyrene beads in mixed solvents

Tomáš Kužela[a,*], Martin Burdík[b], Pavel Kaloda[a], Kristýna Kalodová[a], Dušan Fojtů[c], Petr Elisek[a], Josef Hrnčiřík[a], Roman Jašek[b], Marek Ingr[a]

[a]*Faculty of Technology, Department of Physics and Materials Engineering, Tomas Bata University in Zlín, Nám. T.G. Masaryka 5555, 76001 Zlín, Czech Republic*

[b]*Faculty of Applied Informatics, Department of Informatics and Artificial Intelligence, Tomas Bata University in Zlín, Nad Stráněmi 4511, 760 05 Zlín, Czech Republic*

[c]*Faculty of Applied Informatics, Department of Computer and Communication Systems, Tomas Bata University in Zlín, Nad Stráněmi 4511, 760 05 Zlín, Czech Republic*

[*]*Corresponding author. E-mail address: tl_kužela@utb.cž (T. Kužela).*

Abstract

Optical traps are devices used to micromanipulation microscopic objects using a focused laser beam in an optical microscope field of view. Trapping such objects is possible only when their refractive index is higher than the environment's. Typically, trapping experiments are carried out in aqueous solutions, exploiting the low refractive index of water. Experiments in different pure organic solvents were also reported, showing not very good dependence of the optical-trap force constant on the solvent refractive index. In this study, we carry out optical trapping experiments in mixed water:organic solvents where the organic components are dimethyl sulfoxide, ethylene glycol, and glycerol. Trends of corner frequencies measured in these mixtures follow the theoretical calculations well for all the studied systems in the whole molar-fraction range, indicating their dominant dependence on the refractive index. The conversion of the corner frequencies to the force constants of the trap is strongly influenced by the differences in viscosity throughout the molar-fraction range that emphasizes experimental errors in the regions where it is high. In addition, the force-constant and corner-frequency curves can serve as an indicator of ideality of the potential profile of the optical trap.

Keywords: Optical tweezers, mixed solvent, dimethyl sulfoxide, ethylene glycol, glycerol, trap stiffness

1. Introduction

Optical trap (or optical tweezers) is an optical microscopy-based micromanipulation device enabling the manipulation of microscopic objects and measurement of microscopic forces acting on them [**1**]. This predestines them to many applications in a wide range of scientific subjects from physics to biology [**2**]. Optical traps work on the principle of the momentum change of the photons of the incident laser beam focused on the trapped object. The individual rays of the laser beam are refracted by this object, changing thus their momentum, therefore the difference between their final and initial

momentum is received by the object itself (Fig. 1). Optical trapping is possible only when the refractive index of the object is higher than that of the environment. In this case, the object is always attracted towards the focal point of the beam.

The strength of an optical trap can be measured by a force constant analogous to that of the linear spring since the force produced by the trap on the trapped object in the local surrounding of the equilibrium position of the object in the trap is linearly proportional to the distance of the object from this position. The equilibrium position is shifted from the laser-beam focus by a small distance in the direction of the beam propagation due to the influence of the reflected photons. Obviously, the force constant depends on the refractive index of the environment (considering a given refractive index of the object). Some previous studies showed [**3,4**] that the dependence of the force constant on the refractive index need not be monotonous. It may reach its maximum for a certain refractive index value and decrease in both directions from this value.

Optical tweezers are most often used in biophysical experiments where they serve as a tool for the micromanipulation of biomolecules, mostly proteins and nucleic acids, attached to polystyrene (PS) beads of microscopic dimensions, typically in the pm order of magnitude [**1,5**]. Trapping these beads enables the mechanical deformation of these molecules and thus studying phenomena like protein unfolding [**6-9**] or DNA-duplex dissociation [**10-13**]. It can also be used for hindering the motion of molecular motors and studying their functions at varying force loads [**14-17**]. Most importantly, the microscopic single-molecule forces playing roles in the mentioned processes can be measured with the pN-nN precision. In these experiments, water and diluted aqueous solutions serve as the environment of the PS beads because of their biocompatibility with the biomolecules. Nevertheless, optical trapping is also possible in different solvents, as shown by Black et al. [**18,19**].

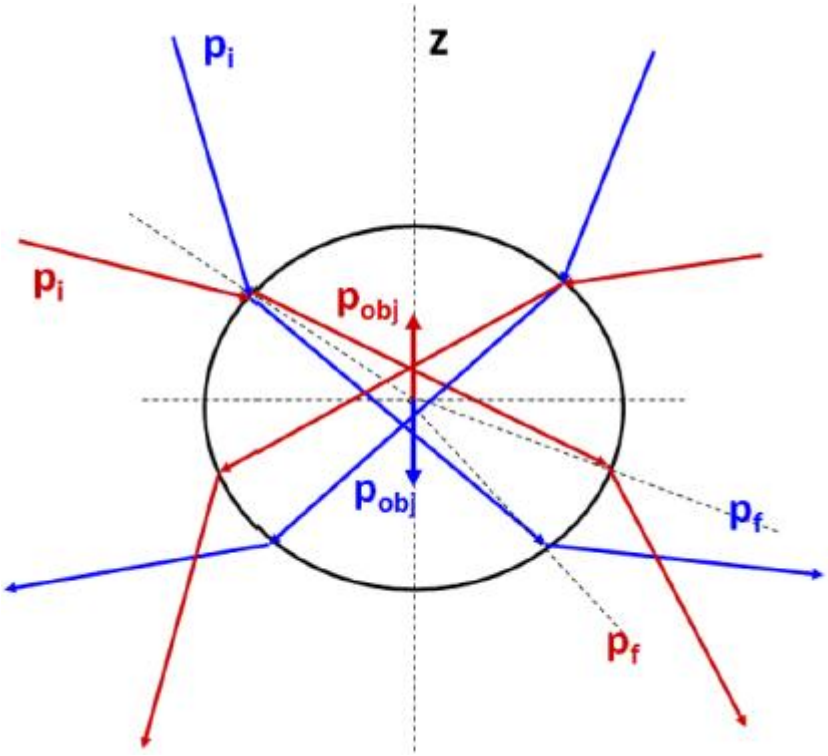

Fig. 1. A scheme of the rays causing the optical trapping. Blue rays - the focal point of the laser beam is below the center of the bead - the bead is pushed forward. Red rays - the focal point is above the center - the bead is pulled backwards. Initial and final vectors of the momentum of the photons are denoted as p_i and p_f, the momentum received by the trapped object is p_{obj}. A similar construction can be done even when the center is out of the z-axis, the center is always pulled towards the focus.

In that study, optical trapping of PS beads covered with a fused silica layer, protecting the bead from dissolution, was carried out. Surprisingly, not many differences were identified between individual solvents, therefore the refractive-index dependence of the force constant was not observed.

This study is aimed at investigation of the properties of optical trapping of spherical PS beads in mixed solvents consisting of water and an organic liquid miscible with it. Varying ratios of their components provide continuous changes of the refractive index of the solvent, but also its viscosity. Viscosity does not affect the force constant of the trap but has a direct influence on the dynamics of the trapped bead. The oscillations of the bead around the equilibrium position in the trap get slower when the viscosity of the environment grows, therefore viscosity must be known when the force constant is measured using the frequency analysis of the force spectrum of the trap.

To our knowledge, a systematic study of the force-constant dependence on the composition of mixed solvents has not been carried out yet. In spite of that, studying these systems may be interesting for several reasons. The mixed solvents may sometimes provide a better-tuned environment for certain. Furthermore, beads coated with special polymer coatings may cause the local separation of the mixed solvent, which may influence the dynamic behavior of the trapped bead depending on the mixed-solvent composition. This may, in turn, be exploited to study the interaction of mixed solvents with different polymers, which may provide valuable information for the design of environments for the synthesis and processing of advanced polymeric materials. Finally, local solvent separation may be interesting even from the point of view of the basic theory of optical trapping since it allows us to study a bead in an environment of continuously changing refractive index and viscosity.

In this work, we investigate the dynamical behavior of the PS beads in the mixed solvent of water:dimethylsulfoxide ($DMSO$), water: ethylene-glycol (EG) and water:glycerol (GLY). The force constants are determined for a series of concentration ratios and two bead diameters in order to show the dependence of the force constant on the refractive index at different conditions. The study should thus provide the first contribution to the systematic investigation of the phenomenon of optical trapping in mixed solvents.

2. Materials and methods

Polystyrene beads (Sigma-Aldrich, Latex beads, polystyrene, LB8 and LB30) of the diameter of 0.8 μm and 3 μm were used in this study. Before the measurement, the original dispersion was diluted by water 1000 times by the mixed water:organic solvents specified in **Table 1**.

2.1. Experimental device

A device for the formation of dual optical tweezers was constructed in our laboratory on the base of the Olympus IX-73 fluorescent microscope with the oil immersion phase objective 100× with NA 1.40 (UPlanSApo) (**Fig. 2**).

The beam is split into two half-beams which are independently deflected by the piezoelectrically controlled movable mirrors in two perpendicular directions, after which they have merged in the same line again. Afterwards, one bead was trapped using the focused beam of the 3200 mW diode laser of the wavelength of 808 nm. The trap's position is known from the microscope image but is also detected from the waste portion of the primary beam by a quadrant photodiode - QPD (Thorlabs PDQ80A). The reflected light from the trapping object is collected by the objective and leads along the same line as

the primary trapping beam. The reflected beam runs through a projector that projects the focal plane on the plane of the Position Sensing Detector - PSD (Thorlabs PDP90A Lateral Effect Position Sensor). The projection of the micrometer-sized beads is of millimeter size. The PSD detector is aligned so that the projection is centered in the center of the detector's active area. When using both traps simultaneously, blocking one of the optical lines regularly during position detection and determination is necessary. This was carried out by an optical chopper system. Although the device is a dual optical tweezers system in principle, in this study only one optical line was used for trapping just one bead while the other one was blanked permanently.

All data from the detectors are recorded by PC after the A/D conversion carried out by the DAQ board card (OMEGA Engineering, OMB-DAQBOARD-3000 Series card). Controlling the device and data processing are carried out by our own software programmed in $C\#$, some features were coded in Python.

The prepared dispersions were loaded in the homemade microfluidic chips and kept there till the equilibration of the system (equilibration of temperature and vanishing of flow). Our chips were optimized for micromanipulation experiments in optical tweezers device. For this purpose, we designed sandwich construction of coverslip/silicone-rubber poly-dimethyl-siloxane ($PDMS$) film/microscope slide (**Fig. 3**).

Table 1 Stock solutions of mixed solvents ($DMSO$, EG and Glycerol) and their molar and mass fraction.

φ_{org}	w_{DMSO}	x_{DMSO}	w_{EG}	x_{EG}	w_{GLY}	x_{GLY}
0.0	0.00	0.00	0.00	0.00	0.00	0.00
0.1	0.11	0.03	0.11	0.02	0.12	0.03
0.2	0.22	0.06	0.22	0.05	0.24	0.06
0.3	0.32	0.10	0.32	0.09	0.35	0.10
0.4	0.43	0.15	0.43	0.13	0.46	0.14
0.5	0.53	0.20	0.53	0.18	0.57	0.20
0.6	0.62	0.28	0.62	0.25	0.66	0.27
0.7	0.72	0.37	0.72	0.34	0.75	0.37
0.8	0.82	0.51	0.82	0.47	0.84	0.50
0.9	0.91	0.71	0.91	0.66	0.92	0.71
1.0	1.00	1.00	1.00	1.00	1.00	1.00

φ_{org} ⋯ volume fraction of organic component calculated as $\varphi_{org} = V_{org} / (V_{org} + V_{H2O})$. w ⋯ weight fractions of organic component (specified by the index). x ⋯ molar fractions of organic component (specified by the index).

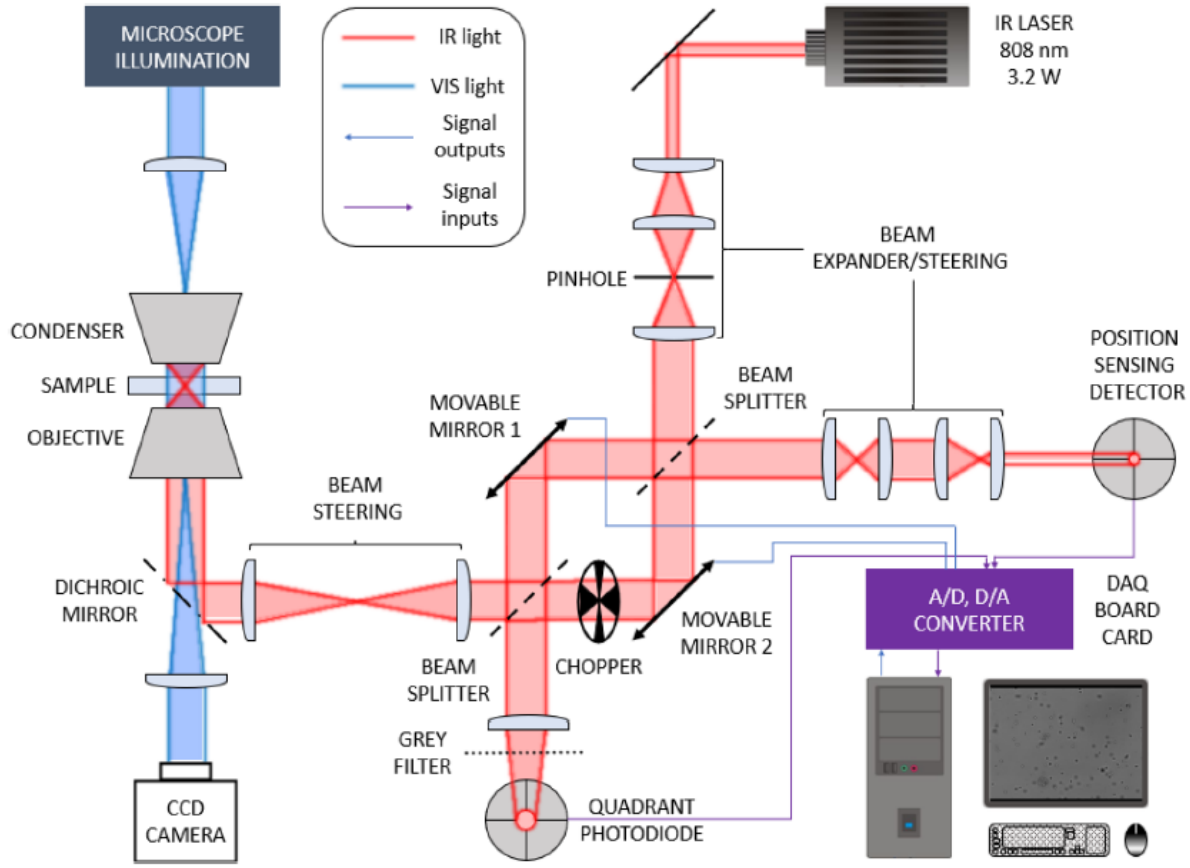

Fig. 2. A scheme of the optical tweezers device generating the dual optical trap.

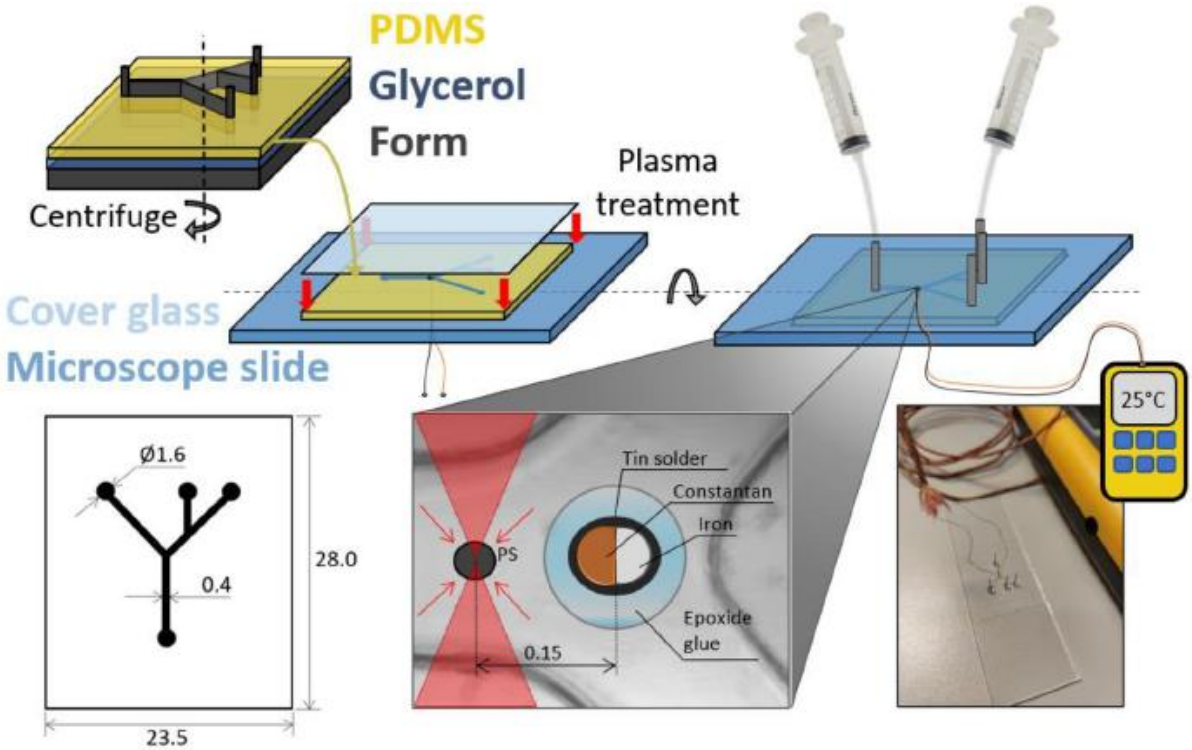

Fig. 3. A scheme of the constructed 3-layer microfluidic chip is stuck using low-temperature oxygen plasma. Thermocouple wires and iron tube connectors are drilled inside the channel and fixed by epoxide glue. The dimensions in the scheme are in milimeters.

The thin $PDMS$ film (approximately 0.1-0.3 mm) with the imprinted shape of the channel (Y-shape with one additive channel) qualify the liquid's area.

The temperature was measured by a thermocouple type J with 76 pm wires (Omega Engineering, inc.) soldered using tin solder with 3 % silver (Broquetas Eco 6). Soldered wires (approximately 20 mm) were inserted into the main channel through a drilled separate hole (0.5 mm) in the microscope slide (close to the measuring area) and fixed by epoxide glue. The PS bead was approximately measured 150 μm far from the thermocouple.

2.2. Mathematical and statistical analysis of acquired data

All data from the detectors were recorded by PC after the A/D conversion carried out by the DAQ board card (OMEGA Engineering, OMB-DAQBOARD-3000 Series card). The optimum acquisition time was determined as 100 s at the sampling frequency of 100 kHz with respect to the power spectrum fitting by the Lorentz function. Shorter time leads to missing low-frequency motions (Fig. SI in Supplementary materials), which makes the evaluation of corner frequency difficult or even impossible. On the other hand, longer acquisition time would lead to processing excessively big amount of data which would complicate the computational processing.

The influence of the proximity of the channel walls in z-direction (between coverslip and microscope slide) on the trapping properties was tested experimentally (see Fig. S2 in Supplementary materials). It can be seen that the PSD signal and subsequently force constant of the trap is influenced when the trap is very close to the coverslip, but from the distance of approx. 3 pm from the base position (the closest position to the coverslip in which the bead can be trapped without being firmly attached to it by the non-covalent interactions) the signals do not vary. Due to the high numerical aperture of the used objective the working distance is short and the imaging, as well as trapping, properties are the best close to the coverslip. Therefore, we carry out our experiments at approx. 4 pm from it. In the plane perpendicular to the optical axis the channel is relatively wide in comparison with the trapped bead and the focal area of the trapping beam, it is even larger than the field of view of the microscope. Therefore, no influence of the channel walls on the trapping properties was expected when the trap is located in the middle of the channel which is the setup used in all experiments.

Experiments in a given system were repeated at least three times, each time with a different bead.

Acquired series of the 3 μm bead positions in the trap as a function of time (**Fig. 4**A) were transformed to the force spectra using the Fast Fourier Transform (FFT) algorithm [**20**] (**Fig. 4**B).

For FFT the algorithm contained in the NumPy library [**21**] was used in our software. The data were fitted by the Lorentz function, and the corner frequency was determined for every such spectrum as described previously [**22,20**].

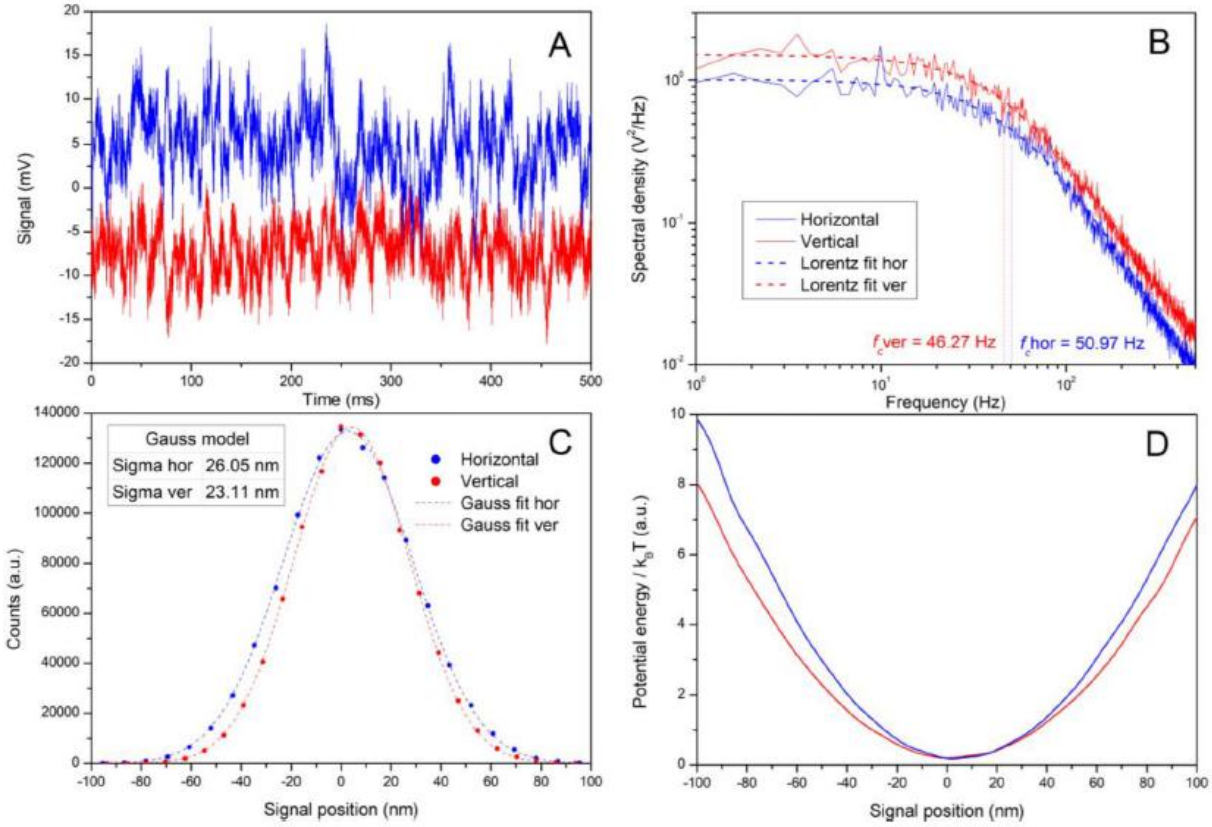

Fig. 4. Measured quantities and characteristics of the optical trap. A, Acquired signals of the 3 μm PS bead position using the PSD as a function of time. B, Force spectrum of the optical trap as a Fourier-transform of the function in panel A with a Lorentz function fit and the point of maximum curvature f_c. C, Frequency of occurrence of the 3 μm PS bead in varying distances recalculated to the real movement of the particle in nm scale from the trap center (position distribution). D, Potential energy in k_BT unit of the trapped 3 μm particle as a function of its distance from the trap center.

The frequency f corresponding to the point of the maximum curvature of this curve called corner frequency (f_c) was determined, and the force constant was calculated as

$$\kappa = 2\pi\gamma_0 f_c, \qquad (1)$$

where y_0 Is the friction coefficient of the trapped particle of a diameter r in environment of the dynamic viscosity n given by the Stokes formula

$$\gamma_0 = 6\pi\eta r. \qquad (2)$$

Once the force constants are determined, the position calibration is done by comparing the standard deviation of the particle position represented by the detector signal (denoted as σ_{V}, in the units of V) with the standard deviation of the position of the bead calculated with the use of the already determined force constant k (σ_{m}, in the units of m). The latter is determined using the following formula [**23**]:

$$\sigma_m^2 = \frac{k_B T}{\kappa}. \qquad (3)$$

The calibration constant δ is then calculated as $\delta = \frac{\sigma_m}{\sigma_V}$. For pure water with trapped 3 μm bead (**Fig. 4**) and the vertical signal the measured aV = 2.80 $\pm$ 0.08 mV corresponds to the $\sigma_m = 24.19 \pm 0.27$ nm, resulting in the calibration constant for vertical axis δ_{ver} = 8.68 $\pm$ 0.34 nm·mV^{-1}. Analogically, $\delta_{\mathrm{hor}} = 6.01 \pm 0.11$ nm·mV^{-1} for the horizontal signal. Actually, this calibration is not necessary for this study, where only the force constants are taken into accounts, but it gives us valuable information about the performance of the device, therefore we mention it here for the completeness of the description.

Furthermore, the distribution function (**Fig. 4**C) of the bead position in the trap can be constructed, and the potential function of the trap can be found using the Boltzmann distribution of energies. The distribution function, i.e. the frequency of occurrence of the bead at the coordinate x, is given by

$$P(x) = \frac{\exp\left(-\frac{V(x)}{k_B T}\right)}{Q}, \tag{4}$$

where $V(x)$ is the trap potential, and Q is a partition function. Hence, the ratio of these frequencies for a point x and the potential minimum x_{min} is

$$\frac{P(x)}{P(x_{min})} = \exp\left(-\frac{V(x) - V(x_{min})}{k_B T}\right). \tag{5}$$

Setting $V(x_{min}) = 0$ we obtain the potential of the trap

$$V(x) = -k_B T \ln \frac{P(x)}{P(x_{min})}. \tag{6}$$

The potential of our generated trap (**Fig. 4**D) given in units of $k_B T$ was calculated using **Eq.** (**6**).

2.3. Viscosity models

Dynamic viscosity $\eta(T)$ of pure solvents as a function of thermodynamic temperature T (water - H_20, ethanol - EtOH, methanol - MeOH) was determined using the simplified version of Vogel-Fulcher-Tammann equation (VFT) [**24**]:

$$\eta(T) = e^{A + \frac{B}{C+T}}, \tag{7}$$

where A, B and C are parameters of Vogel equation for each compound (specified in **Table 2**).

While the viscosity of a pure chemical compound depends only on temperature, the mixed solvent of two miscible liquids also depends on the composition of the solvent. For a given mixture of solvents, experimental values of viscosities for a set of compositions and temperatures were found in the literature [**26-28**]. A linear approximation of viscosity was assigned to every value from this set, which was determined as an average of the viscosities of pure components at the given temperature weighted by the molar fraction:

$$\eta_{lin}(x_{B,\,i},\ T) = \eta_A(T)(1 - x_{B,i}) + \eta_B(T) x_{B,\,i}, \tag{8}$$

where $\eta_A(T)$ and $\eta_B(T)$ are dynamic viscosities of the pure compounds A and B, and x_B, i is the molar fraction of the component B. The index i indicates the individual experimental points of the molar fraction for a given temperature T. Then the excess viscosity was calculated at every measured point as the difference of the experimental viscosity $\eta_{\exp}$ and the linear viscosity:

$$\eta^E(x_{B,\,i},\ T) = \eta_{exp}(x_{B,\,i},\ T) - \eta_{lin}(x_{B,\,i},\ T). \tag{9}$$

The excess viscosity is smooth enough, therefore it can be fitted by a polynomial of an order of 3-6 depending on the given mixture, providing a continuous smooth function $n^E_{fit}(x_B;\ T)$ of x_B with a parameter T. To determine the value of viscosity for a selected temperature within the range covered by the experimental values, we made use of the linear dependence of the logarithm of viscosity lnn of a given liquid on 1 /T (simplified version of **Eq.** (**7**), but accurate enough in the range of interest).

Therefore, for a given x_B a series of $n^E_{fit}(x_B;\ T_j)$ was calculated where T_j are experimental temperatures. Linear regression of this series was calculated, and the obtained equation was used to calculate $\ln\eta^E(x_B; T)$, and subsequently $\eta^E(x_B; T)$, for any temperature from the relevant interval.

Table 2 Vogel equation parameters of pure compounds [**25**].

	A	B	C	T_{min}	T_{max}
H_2O	−3.7188	578.92	−137.546	273	373
EtOH	−7.3715	2770.25	74.6787	159	516
MeOH	−6.7562	2337.24	84.0853	183	463

Finally, the viscosity of the mixture for a given point $[x_B; T]$ was calculated as

$$\eta(x_B, T) = \eta_{lin}(x_B, T) + \eta^E(x_B, T). \tag{10}$$

Fig. 5 shows viscosities and refractive indices of water:organic mixtures at experimental temperature (the exact values of viscosities are shown in Tables S1-S3 in Supplementary material).

2.4. Theoretical simulation of force-constants of optical traps

Force constants of optical tweezers trapping microspheres of different sizes at different solutions were calculated using the model of momentum change of photons running through the microbeads. Two different diameters of the beads were taken into account, 3 μm and 0.8 μm. The calculations were carried out for several values of the refractive index from the studied range of the composition of different mixed solvents. The laser beam was considered as cylindrical of homogeneous intensity throughout its cross section perpendicular to its axis. This beam was considered to be focused to one point by the objective.

The cross section of the beam was covered by a net of grid points located on concentric circles. The number of points on each circle was proportional to its radius to keep the surface related to every point approximately constant. Weights proportional to the precise surfaces of cells related to individual points were assigned to the points.

A sphere characterized by its radius and refractive index was placed to a selected space location. The environment was characterized by its own refractive index, too. The calculation of its path through the sphere was calculated for every ray running through any of the grid points. At both interfaces, when entering and leaving the sphere, the path of the ray was changed in accord with the Snell's law of refraction. Subsequently, the difference between the final and initial momentum vectors of the photon of the considered ray was calculated. An opposite vector, multiplied by the corresponding weight, was attributed to the sphere, and summed with the analogous contributions of all the grid points. The resulting value is proportional to the force acting on the sphere.

This calculation was done in a series of points along the x-axis (perpendicular to the optical axis z) to calculate the whole force profile of the optical trap. The force constant of was calculated as the derivative of the force with respect to x in $x = 0$, i.e. $k = (\frac{dF}{dx})_{x=0}$. This expression of the force constant is only relative because we do not know the exact intensity of the laser beam. Nevertheless, it allows us to compare the force constants among environments of different refractive indices.

3. Results and discussion

3.1. Trap stiffness of PS beads in pure solvents

Corner frequencies and force constants of the optical trap in the selected pure solvents were measured with the 0.8 and 3 μm PS beads at the constant power of the trapping laser and the temperature around 28 °C (specified individually for each measurement and used to calculate the exact viscosity). The results are summarized in **Table 3**, including the viscosities and refractive indices of the solvents. Due to the small anisotropy of the optical trap, the force spectrum was calculated for two dimensions separately, denoted as vertical and horizontal.

The dependence of the force constant on the refractive index of these solvents is not well pronounced. Although $DMSO$, as the solvent with the highest refractive index, provides the lowest force constant, the four other solvents show values changing in a random way in a certain interval. This is not very different from the results of other studies [**18,19**].

This may be caused by imprecise temperature and laser intensity determination in individual experiments. Incorrectness in the temperature causes differences in viscosity that influence the conversion of the measured corner frequency to the force constant rather sensitively, which is the probable cause of the observed randomness in the results.

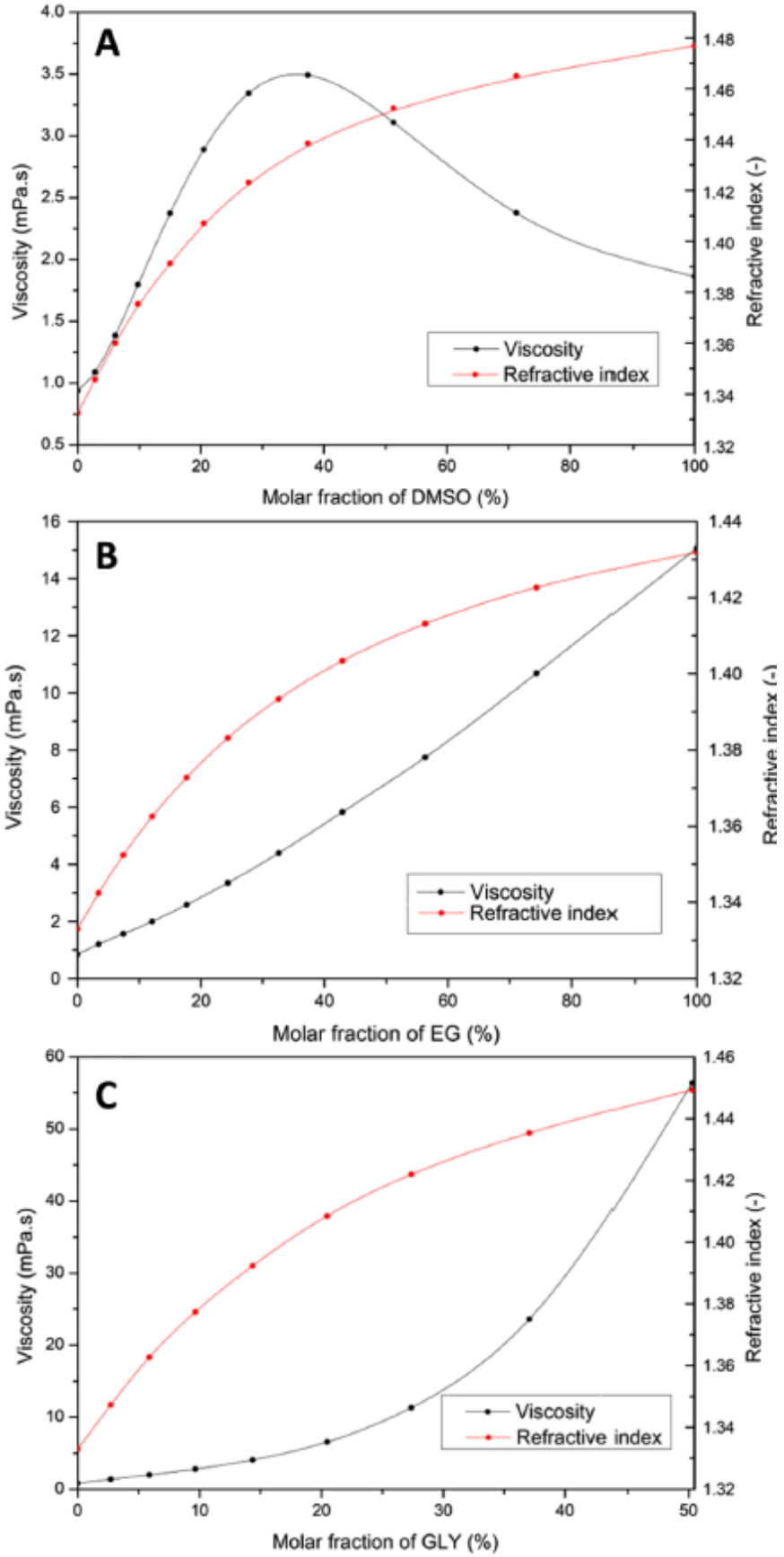

Fig. 5. Viscosity and refractive index as a function of the molar fraction of water:$DMSO$ (a), water:EG (B), and water:GLY (C) mixtures at the experimental temperature.

3.2. Trends of the trap stiffness in the mixed solvents

Measurements of the force constants in the mixed solvent environment were carried out in a temperature range from 24.5 to 30.1 °C (measured individually for each measurement and used to calculate the exact viscosity shown in Tables S1-S3 in Supplementary material) for three systems - water:$DMSO$, water:EG and water:GLY. Volume fraction of the organic component was increased by the steps of 10 vol.% within the whole range from pure water to pure organic component (in case of glycerol only up to 80 % for 3 qm bead and 60 % for 0.8 qm bead) and was subsequently recalculated to molar fraction. Viscosity of the solutions was determined according to the model described in Section 2.3. Vertical and horizontal force spectrum was acquired as described previously.

Table 3 Refractive indices. viscosities. comer frequencies and optical-trap force constants of the used pure solvents. Two latter quantities are measured with 3 μm PS beads.

	Refractive index (-)	Viscosity (mPa.s)	Vertical f_c (Hz)	Horizontal f_c (Hz)	Vertical κ (pN/μm)	Horizontal κ (pN/μm)
H_2O	1.3239	0.90	45.56 ± 0.86	46.00 ± 0.72	7.31 ± 0.15	7.38 ± 0.12
MeOH	1.3314	0.50	80.27 ± 2.14	83.92 ± 0.89	7.16 ± 0.29	7.48 ± 0.03
EtOH	1.3536	1.01	35.88 ± 2.43	32.48 ± 1.33	6.42 ± 0.45	5.81 ± 0.24
EG	1.4319	15.06	2.54 ± 0.14	3.29 ± 0.07	6.80 ± 0.36	8.81 ± 0.25
DMSO	1.4768	1.86	12.07 ± 0.71	9.72 ± 0.41	3.99 ± 0.24	3.22 ± 0.13

For every molar-fraction value, the acquired time dependence of the bead's position was Fourier-transformed to the force spectrum. The corner frequency was determined by the fitting procedure described in **Section 2.2**.

The measured values of the corner frequency and the force constants derived from them are shown in Tables S1-S3 in Supplementary material together with the conditions of the experiments.

The corner frequency continuously decreases in all solvents without substantial noise in the trends. However, the curves of the force constants show various hills and valleys that should not be present in the expected trends. It should be noted that all these deviations are high in the regions where the viscosity is also high. Therefore, it seems that the viscosity, which multiplies the corner frequency in its conversion to the force constant (**Eqs**. (**1**) and (**2**), increases the noise of the measured corner frequencies, deteriorating thus the trends of the dependence of force constant on the molar ratio.

Fig. 6 shows the quantities plotted in Fig. S3 in Supplementary material normalized to their values for pure water. Such curves allow us to compare the experimentally measured values with their theoretically simulated counterparts. The figure shows that the corner frequencies follow the theoretical model with high accuracy for all the studied systems. These trends are disturbed only by random deviations given by small experimental errors. However, these measurements show that the corner frequency strictly obeys the theoretical presumptions based on the knowledge of the refractive indices of both the sphere and the environment and the viscosity of the environment.

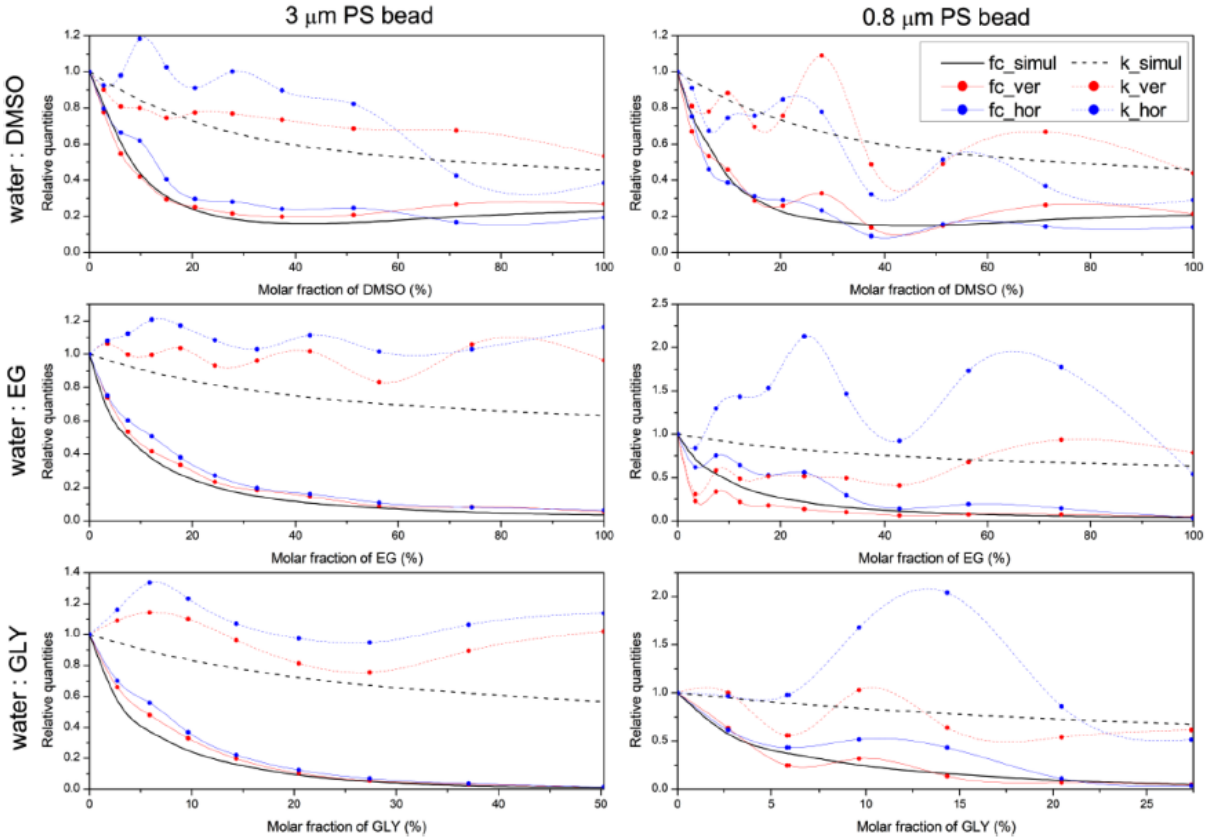

Fig. 6. Relative quantities of corner frequency and trap stiffness of 3 μm (left column) and 0.8 μm (right column) PS bead in studied mixtures. Acronyme "fc" stands for the corner frequency, "k" for the force constant, "ver" and "hor" for vertical and horizontal directions, respectively. Solid and dashed black curves present the results of the theoretical simulations.

The curves representing the force constant are also in approximate agreement with the theoretical assumptions, but their deviations from the ideal trends are relatively large. Qualitatively, the trends of both kinds of curves are in agreement as both the experimental curves, corner frequency, and force constant, are either higher or lower than their theoretical counterparts in every single point. It is, however, obvious that quantitatively, the absolute values of the differences of the force-constant curves exceed those of corner-frequency curves, especially in the regions where the viscosity of the solvent is high. The reason is that the corner frequency is the quantity obtained directly from the experiment that is measured with quite uniform experimental error throughout the whole range of the solution composition. The force constant, on the contrary, is obtained by multiplication of the measured corner frequency, including the experimental error, by the Stokes factor that is proportional to viscosity of the solvent (**Eqs.** (**1**) and (**2**). However, in principle, the force constant is the primary quantity that determines the trap properties, no matter that we cannot measure it directly, and it is independent of viscosity and only mildly varying within the composition range due to the variations of the refractive index. As the viscosity of some mixtures can vary in relatively large extents, the resulting curve of the corner frequency has a considerably more varied profile than the force constant. Therefore, in the regions of high viscosity we measure relatively small corner-frequency values and multiply them by large Stokes factors to obtain the force constant. Together with them, we also multiply the uniform experimental error of corner frequency, which results in a rather high error of the force constant. For instance, the viscosity of the water:GLY solution is rather low at low molar fraction of GLY, while at 50 % (molar) of GLY it is about 50fold larger. Therefore, even the experimental errors will be multiplied by a 50-times larger number which makes the obtained results rather unreliable. Thus, the evaluation of the force constants looks quite reasonable for the

water:$DMSO$ solution, where the difference between the maximum and minimum viscosity is only about 4-fold. EG and GLY mixtures show larger differences and, moreover, grow monotonously along with the organic-component molar fraction. Therefore, the force constants in these mixtures look rather unreliable, especially at the organic-rich end of the molar-fraction range.

Measurements in the mixed solvents clearly show that the measurement of optical-trap force constants is very difficult, especially in high-viscosity solvents. This may explain the results obtained for the pure solvents by us (**Table 3**) and other authors [**18,19**].

While the clearly reproducible trend of corner frequencies indicates a good accuracy of the measurements, the oscillating results show that the determination of the force constant for just one selected solvent may be complicated by several factors. First of all, the random deviations distort the result, especially in the high-viscosity region. Furthermore, the determination of the viscosity can bring some troubles itself. At these measurements, it is sometimes difficult to determine the temperature precisely. However, viscosity is strongly dependent on temperature, which may have a further distorting influence on the obtained results.

On the other hand, the high sensitivity of the corner frequency to force constant conversion to many kinds of small deviations can be exploited as a way of checking the quality of the trapping procedure. When the trapping obeys the theoretical model, the curves of the force constant follow the theoretical prediction well, while the deviations indicate a non-ideal trapping process. It is interesting to compare the results for the smaller and bigger beads of the radii of 0.8 and 3.0 μm, respectively. Although the curves for the small beads contain a lot of noise, it can be clearly seen that they follow the theoretical prediction better than the curves of the bigger beads that are typically shifted above the theoretical curve. The probable reason of this phenomenon is that the small beads are trapped precisely in the focus of the beam, where the paths of the rays are closer to the ideal trajectories. On the contrary, the bigger beads also occupy the space quite far around the theoretical focal point where the trap shape need not have the optimal properties. The potential profile of the trap may partially deviate from the optimum paraboloid shape as a consequence of the non-point laser source. The potential is thus slightly shallower in its minimum and steeper farther from it. This non-ideality has the strongest impact in pure water, where the trapping is the strongest, while in the mixed solvent, it may be wiped by the generally shallower profile of the trap. In contrast to this, the smaller bead is located only in the shallower part of the profile, which may cause a weakening of the trap, but still may have the ideal paraboloid profile and thus also a better agreement with the theoretical curve. This is also supported by relatively lower corner frequencies of the small beads compared to the big ones than expected for the ideal trapping with no energy loss. Thus, the agreement of the theoretical and experimental curves can be used to judge the ideality of the potential profile of the trap.

4. Conclusions

This study investigated the trapping of PS beads by the optical trap in the environment of mixed water:organic solvents. In pure solvents of different refractive indices, the force constant qualitatively corresponds with the difference between the refractive indices of the bead and the environment, but the trend cannot be evaluated because of the experimental errors and because the range of the refractive-indices values is not covered with sufficient density. However, the observed trend looks better than at the previously cited reports [**18,19**].

Continuous coverage of a certain range of refractive indices was allowed by the use of three mixed solvents of water:$DMSO$, water:EG and water:GLY in varying ratios of the components. Here, the

observed corner frequency showed a smooth trend throughout the whole studied range. After the normalization to the value for pure water, it also agreed with the theoretical simulation based on the principle of the momentum change of the photons.

Conversion of the corner frequency to the force constant is somewhat a tricky procedure. Although being formally only a linear transformation, viscosity of the environment plays a role of a multiplication factor. This quantity may change remarkably within the studied range of solvent composition, making the conversion strongly non-linear. This non-linearity then emphasizes the experimental error of the corner-frequency determination, which may deteriorate the expected trends, especially in regions of high viscosity.

Furthermore, trapping of small beads is closer to the ideality than that of the big beads. This may be caused by less ideal shape of the trap at a bigger radius from the focal point, therefore influencing more the bigger beads. The trends of the corner-frequency and force-constant curves can thus serve as an indicator of the ideality of the profile of the optical trap.

References

[1] Bustamante CJ, Chemla YR, Liu S, Wang MD. Optical tweezers in single-molecule biophysics. Nat Rev Methods Prim 2021;1:25. **https://doi.org/10.1038/s43586-021-00021-6**.

[2] Polimeno P, Magazzu A, lati MA, Patti F, Saija R, Esposti Boschi CD, et al. Optical tweezers and their applications. J Quant Spectrosc Radiat Transf 2018;218:131-50. **https://doi.org/10.1016/j.jqsrt.2018.07.013**.

[3] Knoner G, Parkin S, Nieminen TA, Heckenberg NR, Rubinsztein-Dunlop H. Measurement of the index of refraction of single microparticles. Phys Rev Lett 2006;97:157402. **https://doi.org/10.1103/PhysRevLett.97.157402**.

[4] Koyanaka S, Endoh S. The effect of relative refractive index on monosized particle movement under laser radiation pressure. Adv Powder Technol 1999;10:205-21. **https://doi.org/10.1163/156855299X00307**.

[5] Arbore C, Perego L, Sergides M, Capitanio M. Probing force in living cells with optical tweezers: from single-molecule mechanics to cell mechanotransduction. Biophys Rev 2019;11:765-82. **https://doi.org/10.1007/s12551-019-00599-y**.

[6] Bustamante C, Alexander L, Maciuba K, Kaiser CM. Single-molecule studies of protein folding with optical tweezers. Annu Rev Biochem 2020;89:443-70. **https:// doi.org/10.1146/annurev-biochem-013118-111442**.

[7] Wang H, Gao X, Hu X, Hu X, Hu C, Li H. Mechanical unfolding and folding of a complex slipknot protein probed by using optical tweezers. Biochemistry 2019;58: 4751-60. **https://doi.org/10.1021/acs.biochem.9b00320**.

[8] Mukherjee S, Mepperi J, Sahu P, Barman DK, Kotamarthi HC. Single-molecule optical tweezers as a tool for delineating the mechanisms of protein-processing mechanoenzymes. ACS Omega 2023;8:87-97. **https://doi.org/10.1021/ acsomega.2c06044**.

[9] Ritchie DB, Woodside MT. Probing the structural dynamics of proteins and nucleic acids with optical tweezers. Curr Opin Struct Biol 2015;34:43-51. **https://doi.org/ 10.1016/j.sbi.2015.06.006**.

[10] Heller I, Hoekstra TP, King GA, Peterman EJG, Wuite GJL. Optical tweezers analysis of DNA-protein complexes. Chem Rev 2014;114:3087-119. **https://doi. org/10.1021/cr4003006**.

[11] Dame RT, Noom MC, Wuite GJL. Bacterial chromatin organization by H-NS protein unravelled using dual DNA manipulation. Nature 2006;444:387-90. **https://doi. org/10.1038/nature05283**.

[12] Nakauchi H, Maeda M, Kanayama N. Terminal sequence-specific interparticle attraction between DNA duplex-carrying polystyrene microparticles in aqueous salt solution assessed by optical tweezers. Langmuir 2021;37:5573-81. **https://doi. org/10.1021/acs.langmuir.1c00349**.

[13] Kimura Y, Bianco PR. Single molecule studies of DNA binding proteins using optical tweezers. Analyst 2006;131:868. **https://doi.org/10.1039/b600157m**.

[14] YILDIZ A, SELVIN P. Kinesin: walking, crawling or sliding along? Trends Cell Biol 2005;15:112-20. **https://doi.org/10.1016/j.tcb.2004.12.007**.

[15] Ishii Y, Yanagida T. A new view concerning an actomyosin motor. Cell Mol Life Sci 2002;59:1767-70. **https://doi.org/10.1007/PL00012504**.

[16] Leidel C, Longoria RA, Gutierrez FM, Shubeita GT. Measuring molecular motor forces in vivo: implications for tug-of-war models of bidirectional transport. Biophys J 2012;103:492-500. **https://doi.org/10.1016/j.bpj.2012.06.038**.

[17] Woerdemann M, Horner F, Denz C. Structured attachment of bacterial molecular motors for defined microflow induction. Optofluid, Microfluid Nanofluid 2014;1. **https://doi.org/10.2478/optof-2014-0001**.

[18] Black JW, Kamenetska M, Ganim Z. An optical tweezers platform for single molecule force spectroscopy in organic solvents. Nano Lett 2017;17:6598-605. **https://doi.org/10.1021/acs.nanolett.7b02413**.

[19] Yusof MFM, Ayop SK, Supian FL, Juahir Y. Optical trapping of organic solvents in the form of microdroplets in water. Chem Phys Lett 2020;749:137407. **https://doi. org/10.1016/J.CPLETT.2020.137407**.

[20] Berg-S0rensen K, Flyvbjerg H. Power spectrum analysis for optical tweezers. Rev Sci Instrum 2004;75:594-612. **https://doi.org/10.1063/1.1645654**.

[21] Harris CR, Millman KJ, van der Walt SJ, Gommers R, Virtanen P, Cournapeau D, et al. Array programming with NumPy. Nature 2020;585:357-62. **https://doi.org/10.1038/s41586-020-2649-2**.

[22] Tolić-Nørrelykke SF, Schaffer E, Howard J, Pavone FS, Julicher F, Flyvbjerg H. Calibration of optical tweezers with positional detection in the back focal plane. Rev Sci Instrum 2006;77:103101. **https://doi.org/10.1063/1.2356852**.

[23] Morgan IL, Saleh OA. Tweezepy: a Python package for calibrating forces in singlemolecule video-tracking experiments. PLoS One 2021;16:e0262028. **https://doi. org/10.1371/JOURNAL.PONE.0262028**.

[24] Tammann G, Hesse W. Die Abhangigkeit der viscositat von der temperatur bie unterkuhlten flussigkeiten. Z Anorg Allg Chem 1926;156:245-57. **https://doi.org/ 10.1002/zaac.19261560121**.

[25] Liquid dynamic viscosity calculation by vogel equation (Water) n.d. **http://ddbonline.ddbst.de/VogelCalculation/VogelCalculationCGI.exe?component=Water** [Accessed 6 July 6, 2023].

[26] LeBel RG, Goring DAI. Density, viscosity, refractive index, and hygroscopicity of mixtures of water and dimethyl sulfoxide. J Chem Eng Data 1962;7:100-1. **https:// doi.org/10.1021/je60012a032**.

[27] Fogg ET, Hixson AN, Thompson AR. Densities and refractive indexes for ethylene glycol-water solutions. Anal Chem 1955;27:1609-11. **https://doi.org/10.1021/ ac60106a033**.

[28] Takamura K, Fischer H, Morrow NR. Physical properties of aqueous glycerol solutions. J Pet Sci Eng 2012;98-99:50-60. **https://doi.org/10.1016/j. petrol.2012.09.003**.